CrossMark

Pancreatic neuroendocrine tumors: MR imaging features preoperatively predict lymph node metastasis

Haitao Sun[1,2] · Jianjun Zhou[3] · Kai Liu[3] · Tingting Shen[3] · Xingxing Wang[4] · Xiaolin Wang[1,2]

Abstract

Purposes Predictive factors of lymph node metastasis (LNM) in pancreatic neuroendocrine tumors (pNETs) are not well established. We sought to identify the value of MR imaging features in preoperatively predicting the lymph node metastasis of pNETs.

Materials and methods In this study, we enrolled 108 consecutive patients with pNETs between January 2009 and June 2018. MR morphologic features and quantitative data were evaluated. Predictors of LNM were evaluated using univariate and multivariate logistic regression models.

Results A total of 108 patients with pNETs were finally enrolled, including 82 LNM-negative and 26 LNM-positive patients. Features significantly related to the LNM of pNETs at univariate analysis were tumor size > 2 cm ($P = 0.003$), Ki-67 > 5% ($P = 0.002$), non-enhancement pattern ($P < 0.001$), apparent diffusion coefficient value ($P < 0.001$), main pancreatic duct dilation ($P < 0.001$) and pancreatic atrophy ($P = 0.032$) and extrapancreatic tumor spread ($P = 0.001$), CNRs during arterial, portal and delay phase ($P = 0.005$, 0.047, and 0.045, respectively), and histological classification ($P = 0.006$). At multivariate analysis, non-enhancement pattern ($P = 0.019$; odds ratio, 6.652; 95% CI 1.369, 32.321) and main pancreatic duct dilation ($P = 0.018$; odds ratio, 6.745; 95% CI 1.379, 32.991) were independent risk factors for predicting the LNM of pNETs.

Conclusion The non-enhancement characteristic and main pancreatic duct dilation appear to be linked with LNM in pNETs. These radiological predictors can be easily obtained preoperatively, and may help to avoid missing pNETs with a high risk of LNM.

Keywords Neuroendocrine tumors · Pancreas · Lymph node metastases · MR imaging

✉ Xiaolin Wang
fduwangxiaolin@hotmail.com

1 Shanghai Institute of Medical Imaging, No. 180 Fenglin Road, Xuhui District, Shanghai 200032, China

2 Department of Interventional Radiology, Zhongshan Hospital, Fudan University, No. 180 Fenglin Road, Xuhui District, Shanghai 200032, China

3 Department of Radiology, Zhongshan Hospital, Fudan University, No. 180 Fenglin Road, Xuhui District, Shanghai 200032, China

4 Department of Pathology, Zhongshan Hospital, Fudan University, No. 180 Fenglin Road, Xuhui District, Shanghai 200032, China

Introduction

Pancreatic neuroendocrine tumors (pNETs) are uncommon, accounting for only 1–2% of all pancreatic malignancies [1]. In recent years, the presence of pNETs has been unceasingly increasing, mainly due to improvements in diagnostic imaging methods, such as computed tomography (CT), magnetic resonance imaging (MRI) and ultrasound (US) [2]. The biological behaviors and clinical outcomes of pNETs are variable and heterogeneous. Although the majority of pNETs have a more indolent nature and longer overall survival (OS) compared to other pancreatic malignant tumors, the postoperative recurrence of pNETs is not rare.

According to the European Neuroendocrine Tumor Society (ENETS) TNM staging system and the American

Joint Committee on Cancer (AJCC) cancer staging system [3, 4], lymph node metastasis (LNM) has been regarded as a definite poor prognostic factor affecting tumor recurrence for patients with pNETs after surgery. Surgical resection has been considered the definitive curative treatment, but this procedure can be linked with postoperative complications in up to 30% of cases. The operative approach varies from tumor enucleation with or without lymphadenectomy to standard resection (i.e., pancreatectomy or pancreaticoduodenectomy), and optimal surgical procedures have not yet been established, partly owing to the dilemma of preoperatively predicting LNM [5]. Therefore, the identification of reliable predictors of LNM in pNETs is of important significance for guiding clinical treatment decisions and avoiding overtreatment in low-risk patients.

At present, the gold standard for judging LNM is still determined using histopathological assessment after resection, and noninvasive preoperative prediction of LNM remains difficult. Preoperative factors predictive of lymph node involvement are not well established, and there are no unequivocal data in the literature indicating which laboratory measures, radiological features, or patient characteristics may be able to predict LNM. Although several clinical predictors of LNM, such as tumor size and Ki-67 index, have been reported, controversy still remains. Moreover, few studies have used radiologic methods to predict the postoperative recurrence of pNETs. In fact, most studies have focused on the radiologic assessment for pNET diagnosis, characterization and staging, whereas the radiologic evaluation of LNM in pNETs has been ignored [6, 7]. MR imaging analysis with diffusion-weighted imaging (DWI) can noninvasively assess the pancreatic parenchyma, neighboring soft tissues, microvascular invasion, and water diffusion behavior in one examination [8]. The purpose of our study was to evaluate the potential role of conventional MR findings, including DWI, in the preoperative prediction of LNM in pNETs.

Materials and methods

Patients

Between January 2009 and June 2018, a total of 284 patients with pathologically confirmed pancreatic pNETs at surgery were reviewed through our hospital pathologic database. This mono-institutional retrospective study included patients who fulfilled the following criteria (Fig. 1): (a) patients who underwent preoperative contrast-enhanced MR examinations, including DWI performed within 2 months prior to surgery, (b) patients with optimal quality MR images without any severe artifacts or motion, and (c) patients who did not undergo local or systemic

treatment prior to surgery. A total of 176 patients were excluded for the following: (a) lack of MRI and ADC images ($n = 126$), (b) poor-quality MR images with any severe motion or artifacts ($n = 6$), (c) lesions too small to characterize on MR images (< 5 mm) ($n = 3$), (d) undergoing local or systemic treatment prior to MRI and surgery ($n = 13$), and (e) lack of lymph node specimens ($n = 28$). Patients who did not receive IV contrast due to allergy or renal issues were also excluded. A total of 108 patients with histopathologically diagnosed pNETs were included in this study. Seventeen patients (15.7%) were functioning (15 insulinomas, 1 gastrinoma, and 1 VIPoma). Two patients presented with multifocal pNETs and 106 patients with unifocal pNETs. For two patients with multifocal lesions, the largest tumor was analyzed in our study. This study was approved by the Institutional Review Board of Zhongshan Hospital, and the requirement for informed consent was waived.

Image interpretation

All patients included in this study underwent dynamic contrast-enhanced MRI of the pancreas performed with 1.5T or 3.0T systems. All patients were positioned supine and imaged with a dedicated phased-array body coil. Baseline pancreatobiliary MR sequences included T1-weighted in-phase and opposed-phase spoiled three-dimensional gradient-echo sequences and axial T2-weighted fat-suppressed 2D turbo-spin-echo (TSE) and diffusion-weighted imaging adopting a single-shot echoplanar imaging pulse sequence with b values of 0 and 500 s/mm^2 using a respiratory triggering. Dynamic MR imaging was performed one time prior to and three times after the intravenous administration of gadopentetate dimeglumine (Magnevist; Bayer HealthCare, Berlin, Germany, 0.1 mmol/kg) at a rate of 2 mL/s with a transverse and coronal breath-hold T1-weighted three-dimensional volumetric interpolated body examination sequence. The injection was immediately followed by a 30 mL of saline flush via a power injector (Spectris; Medrad, Pittsburgh, PA, USA). Acquisitions were performed at 14, 90, and 180 s after contrast administration during the hepatic arterial, portal, and delayed phases, respectively. All parameters for the MR sequences of the two devices are summarized in Table 1.

MR imaging analysis

For the morphological features, the observers measured the tumor size (maximal diameter), tumor margins (well-defined/ill-defined), and location (head/neck, body, or tail). The signal intensity (SI) on the T2-weighted image and the SI at each phase after contrast administration were graded

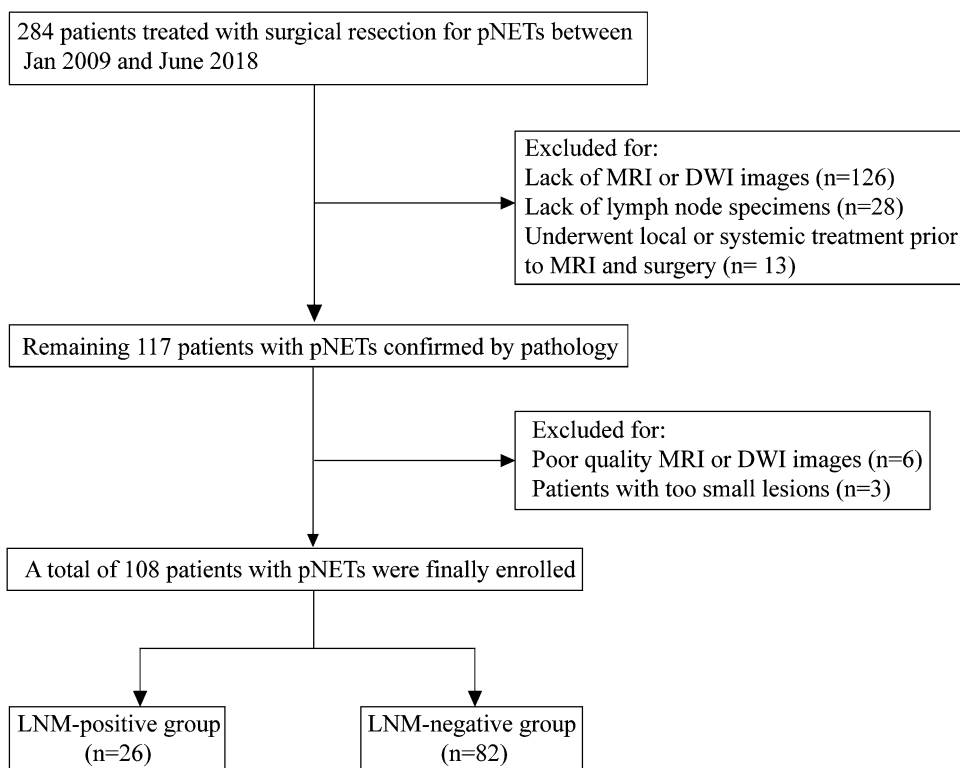**Fig. 1** Flow diagram showing inclusion and exclusion criteria for the study

Table 1 MR acquisition parameters

Parameters	T1-weighted imaging		T2-weighted imaging		Diffusion-weighted imaging		Postcontrast T1-weighted imaging	
	1.5T	3.0T	1.5T	3.0T	1.5T	3.0T	1.5T	3.0T
Repetition time (msec)	6.87	207	2400	2800	5100	3300	3.47	4.07
Echo time (msec)	2.38/4.76	2.31/3.74	94	83	55	70	1.36	1.43
Slice thickness (mm)	4	5.5	6	5.5	6	7	3.5	3
N excitations	1	1	1	1	2	2	5	5
Field of view (mm^2)	297 × 380	275 × 400	309 × 380	295 × 400	285 × 380	313 × 400	380 × 380	309 × 380
Scan matrix	144 × 256	285 × 512	384 × 218	165 × 320	84 × 128	128 × 80	320 × 195	200 × 352
Bandwith(Hz/pixel)	430	930	260	260	1562	2442	400	390
iPAT factor	2	2	2	2	2	2	3	2

The 3.0T imager was a Verio (Siemens Medical Solutions, Erlangen, Germany) unit. The 1.5T imager was a Aera (Siemens Medical Solutions, Erlangen, Germany) unit. Echo times in T1-weighted Imaging included both in-phase and out-phase imagings

as (a) hyperintense, (b) isointense and (c) hypointense relative to the surrounding pancreatic parenchyma. The enhancement degree was defined as two patterns: (a) enhancement (hypervascular on arterial phase compared to surrounding normal pancreas parenchyma) and (b) non-enhancement (iso- or hypovascular on arterial phase compared to surrounding normal pancreas parenchyma). Accompanying findings included tumor texture, the presence of main pancreatic duct dilation (MPDD), the presence of pancreatic atrophy and the presence of

extrapancreatic tumor spread. Main pancreatic duct dilation was defined as a diameter of 3 mm or greater [9]. Tumor texture was divided into solid, solid and cystic, and cystic, which were defined as follows: (a) solid, an enhancing solid portion of more than 90% of the tumor; (b) solid and cystic, an enhancing solid portion of 20–90% of the tumor; and (c) cystic, an enhancing solid portion of less than 20% of the tumor. The abdominal images were interpreted on a PACS workstation by two radiologists

(H.T.S. and J.J.Z., with 8 and 30 years of experience in abdominal imaging, respectively) in a blinded manner.

ADC was calculated according to a mono-exponential fit of the signal intensity using $b = 0$ and 500 s/mm^2. In addition, The contrast-to-noise ratios (CNRs) were calculated as CNR = $(SI_{le} - SI_{pe})/SI_m$, where SI_{le} represents the signal intensity of the tumor on enhanced images, SI_{pe} represents the signal intensity of normal pancreatic parenchyma on enhanced images, and SI_m is the signal intensity of the paraspinal muscle. All regions of interest (ROIs) were manually drawn in the center of the tumor and encompassed at least two-thirds of its solid component, and necrosis, hemorrhage, vessels, and cystic textures were avoided. Quantitative analysis of the lesions was performed by two radiologists (H.T.S and K.L.), and the average value was used for analysis.

Histopathologic analysis

All patients with pNETs underwent surgical resection. Histopathologic findings from resected specimens were analyzed by one pathologist specialized in pancreatic pathology (X.X.W.). According to the 2010 WHO classification, all lesions were classified as G1 (< 2 mitoses/10 high power fields (HPF) and/or a Ki-67 index $\leq$ 2%); G2, (2–20 mitoses/10 HPF) and/or 3% < Ki-67 $\leq$ 20%) and G3, (> 20 mitoses/10 HPF) and Ki-67 index > 20%). Lymphatic invasion and microscopic venous and perineural infiltration were evaluated via immunostaining for CD31 and D2-40 as described previously [10].

Statistical analysis

The distributions of continuous variables are expressed as the mean $\pm$ standard deviation (SD) and medians (interquartile range [IQR] = 25–75). Categorical variables are presented as numbers and percentages. Continuous variables were compared between LNM-positive and LNM-negative of pNETs with Student's t test or the Mann–Whitney U test. Categorical variables were compared between two groups using Pearson's Chi squared test or Fisher's exact test. Univariate and multivariate logistic regression analysis was performed to identify independent factors of LNM. Receiver operating characteristic (ROC) curve analysis was performed to test the performance in diagnostically distinguishing between two groups. For parameters that were statistically significant in the multivariate logistic regression, we calculated the sensitivity, specificity, cut-off value, and area under the ROC curve (AUC). The optimal cut-off value was defined as the point that yielded the best sensitivity and specificity for differentiation. Interobserver variability of the qualitative image analysis was assessed by means of κ statistics. The strength

of agreement was assessed as poor if $\kappa < 0.20$, fair if $\kappa = 0.21–0.40$, moderate if $\kappa = 0.41–0.60$, good if $\kappa = 0.61–0.80$ and excellent if $\kappa = 0.81–1.00$. All statistical analyses were performed using SPSS (version 22, IBM, Armonk, NY, USA) and GraphPad Prism version 7 (GraphPad Software, Inc, San Diego, CA), Differences with P values less than 0.05 were considered significant.

Results

Baseline characteristics

The clinical data for 108 pNETs are shown in Table 2. A total of 108 patients (median age, 55.9 years; range 19–79 years) with pNETs were finally included, including 47 (43.5%) men (median age, 55.3 years; range 21–79 years) and 61 (56.5%) women (median age, 56.4 years; range 19–79 years) who were LNM-positive ($n = 26$) and LNM-negative ($n = 82$) according to the pathohistological examination. In our study cohort, seventeen patients (15.7%) had functional tumors (15 insulinomas, 1 gastrinoma, and 1 VIPoma). 2 patients had multifocal lesions, and 106 patients had only one lesion. According to the 2010 WHO classification, there were 37 G1 tumors (34.3%), 59 G2 tumors (54.6%), and 12 G3 tumors (11.1%).

Comparison of the clinicopathological features between LNM-positive and LNM-negative pNETs

Clinicopathological features of all patients are summarized in Table 2. The age of the patients was similar between the LNM-negative group (56.85 $\pm$ 2.87 years) and the LNM-positive group (55.86 $\pm$ 13.1 years) ($P = 0.527$). The LNM-positive group showed a larger size (> 2 cm) (92.3% [24 of 26] vs. 54.9% [45 of 82], $P < 0.001$), a higher Ki-67 index (> 5%) (57.7% [15 of 26] vs 24.4% [20 of 82], $P = 0.003$), and a higher WHO classification (G2-3) (88.46% [23 of 26] vs 58.5% [48 of 82], $P = 0.006$) more frequently than the LNM-negative group. However, tumor margin, location, and type of function showed no significant differences between the LNM-positive and LNM-negative pNETs groups (all $P > 0.05$) (Table 2).

Comparison of the radiological features between LNM-positive and LNM-negative pNETs

The MR findings for all LNM-positive and LNM-negative pNETs are summarized in Table 3. Compared with lesions without LNM, the lesions with LNM showed more frequent non-enhancement (69.2% [18 of 26] vs. 21.9% [18 of 82], $P < 0.001$) (Figs. 2a, 3), pancreatic atrophy (50.0%

Table 2 Analysis of clinicopathological characteristics for the relationship with lymph node metastasis (LNM) of pNETs

Parameter	LNM		P value
	Negative (n = 82)	Positive (n = 26)	
Age (year)[a]	56.85 ± 2.87	55.86 ± 13.1	0.527
Location			0.716
Head	37 (45.12%)	14 (53.85%)	
Body	13 (15.85%)	3 (11.54%)	
Tail	32 (39.02%)	9 (34.62%)	
Tumor size			< 0.001
≤ 2 cm	37 (45.12%)	2 (7.69%)	
> 2 cm	45 (54.88%)	24 (92.31%)	
Ki-67			0.003
≤ 5%	62 (75.61%)	11 (42.31%)	
> 5%	20 (24.39%)	15 (57.69%)	
Type of function			0.152
Non-functioning	65 (79.27%)	24 (92.31%)	
Functioning	17 (20.73%)	2 (7.69%)	
Histological classification			0.006
G1	34 (41.46%)	3 (11.54%)	
G2	42 (51.22%)	17 (65.38%)	
G3	6 (7.32%)	6 (23.08%)	

Unless otherwise indicated, data are numbers of lesions, with percentage in parentheses

[a]Data are reported as means ± standard deviations

[13 of 26] vs. 15.8% [13 of 82], $P = 0.001$) and main pancreatic duct dilation (50.0% [13 of 26] vs. 10.9% [9 of 82], $P = 0.005$) (Figs. 2b, 3). However, other qualitative MR features, including T2-weighted image signals, tumor texture, signal on portal and delay phases, pancreatic atrophy and extrapancreatic tumor spread showed no significant differences between the two groups (all $P > 0.05$) (Table 3).

In the quantitative MR findings analysis, the ADC values for pNETs without LNM (1.72 [1.29, 2.07] $\times 10^{-3}$ mm^2/s) were significantly higher than those for pNETs with LNM (1.15 [0.96, 1.50] $\times 10^{-3}$ mm^2/s) ($P < 0.001$). In addition, the CNRs for the LNM-negative groups during the arterial phase (0.16 [− 0.45, 0.42] vs. − 0.34 [− 0.71, 0.19]), portal phase (0.17 [− 0.49, 0.46] vs. 0.46 [− 0.33, 0.16]) and delay phase (0.23 [0.05, 0.43] vs 0.04 [− 0.21, 0.26]) were significantly higher than those for the LNM-positive groups (all $P < 0.05$) (Table 3).

Independent risk factors for MR findings in differentiating LNM-positive and LNM-negative pNETs

Table 4 shows the several risk factors that were found to be significantly related to the LNM of pNETs at univariate analysis, including tumor size > 2 cm, Ki-67 > 5%, histological classification, enhancement pattern, presence of

pancreatic atrophy and extrapancreatic tumor spread, presence of main pancreatic duct dilation, ADC value and CNR during the arterial, portal and delay phases. The other parameters were not significantly different between the two groups. At multivariate stepwise logistic regression analysis, however, only the non-enhancement pattern ($P = 0.019$; odds ratio, 6.652; 95% CI 1.369, 32.321) and main pancreatic duct dilation ($P = 0.018$; odds ratio, 6.745; 95% CI 1.379, 32.991) were independent indicators for differentiating the LNM of pNETs (Fig. 4). Figure 5 shows the receiver operating characteristic curve of the enhancement degree and MPDD. The sensitivity, specificity, and area under the receiver operating characteristic curve of non-enhancement degree and MPDD were 69.23%, 78.05%, 0.736 and 50.00%, 89.02%, 0.695, respectively.

Interobserver agreement in LNM-positive and LNM-negative pNETs

The two observers in our study showed excellent interobserver agreement for tumor margin ($\kappa = 0.853$) and presence of MPDD ($\kappa = 0.943$) and the classification of the enhancement degree ($\kappa = 0.917$), presence of pancreatic atrophy ($\kappa = 0.837$), signal in T2-weighted images ($\kappa = 0.865$), and signals on portal and delay phases

Table 3 Analysis of radiological features for the relationship with lymph node metastasis (LNM) in pNETs

Parameter	LNM		P value
	Negative (n = 82)	Positive (n = 26)	
Tumor texture			0.208
Cystic	5 (6.1%)	4 (15.38%)	
Solid	68 (82.93%)	21 (80.77%)	
Solid and cystic	9 (10.98%)	1 (3.85%)	
Tumor margin			0.925
Well-define	70 (85.37%)	22 (84.62%)	
Ill-define	12 (14.63%)	4 (15.38%)	
Signal in T2-weighted images			0.248
Hyperintense	61 (74.39%)	15 (57.69%)	
Hypointense	7 (8.54%)	3 (11.54%)	
Enhancement pattern			< 0.001
Enhancement	64 (78.05%)	8 (30.77%)	
Non-enhancement	18 (21.95%)	18 (69.23%)	
Signal on portal phase			0.391
Hyperintense	50 (60.98%)	12 (46.15%)	
Isointense	22 (26.83%)	9 (34.62%)	
Hypointense	10 (12.2%)	5 (19.23%)	
Signal on delay phase			0.424
Hyperintense	51 (62.2%)	13 (50%)	
Isointense	20 (24.39%)	7 (26.92%)	
Hypointense	11 (13.41%)	6 (23.08%)	
Presence of MPDD	9 (10.98%)	13 (50%)	< 0.001
Presence of pancreatic atrophy	10 (12.2%)	8 (30.77%)	0.027
Presence of extrapancreatic tumor spread	13 (15.85%)	13 (50%)	0.001
ADC ($\times 10^{-3}$ mm^2/s)[a]	1.72 (1.29, 2.07)	1.15 (0.96, 1.50)	< 0.001
CNR during the arterial phase[a]	0.16 (− 0.45, 0.42)	− 0.34 (− 0.71, 0.19)	0.005
CNR during the portal phase[a]	0.17 (− 0.49, 0.46)	− 0.46 (− 0.33, 0.16)	0.005
CNR during the delay phase[a]	0.23 (0.05, 0.43)	0.04 (− 0.21, 0.26)	0.012

Unless otherwise indicated, data are numbers of lesions, with percentage in parentheses

ADC apparent diffusion coefficient, *CNR* Contrast-to-noise ratio, *MPDD* main pancreatic duct dilation, *IQR* inter-quartile range

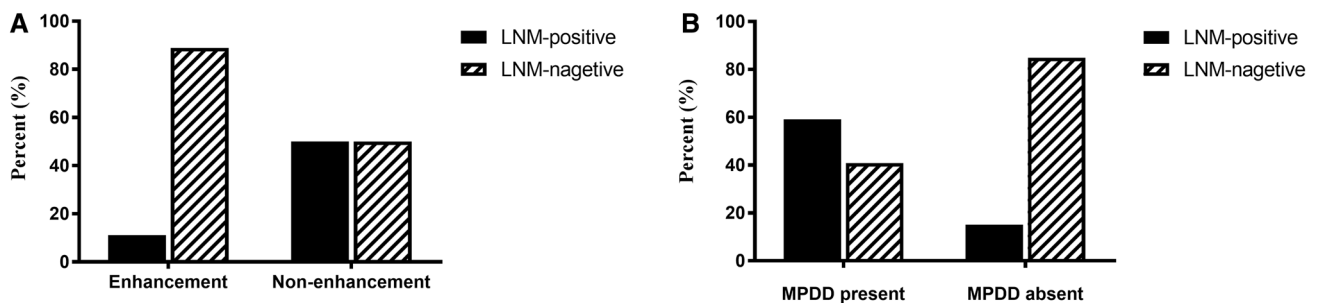[a]Data are reported as medians (IQR 25–75)

Fig. 2 Relation between the lymph node metastasis of pNET and **a** the presence of MPDD, **b** enhancement pattern. The lesions with LNM showed more frequent non-enhancement (69.2% [18 of 26] versus 21.9% [18 of 82], P < 0.001), and MPDD (50.0% [13 of 26] versus 10.9% [9 of 82], P = 0.005) compared with those without LNM
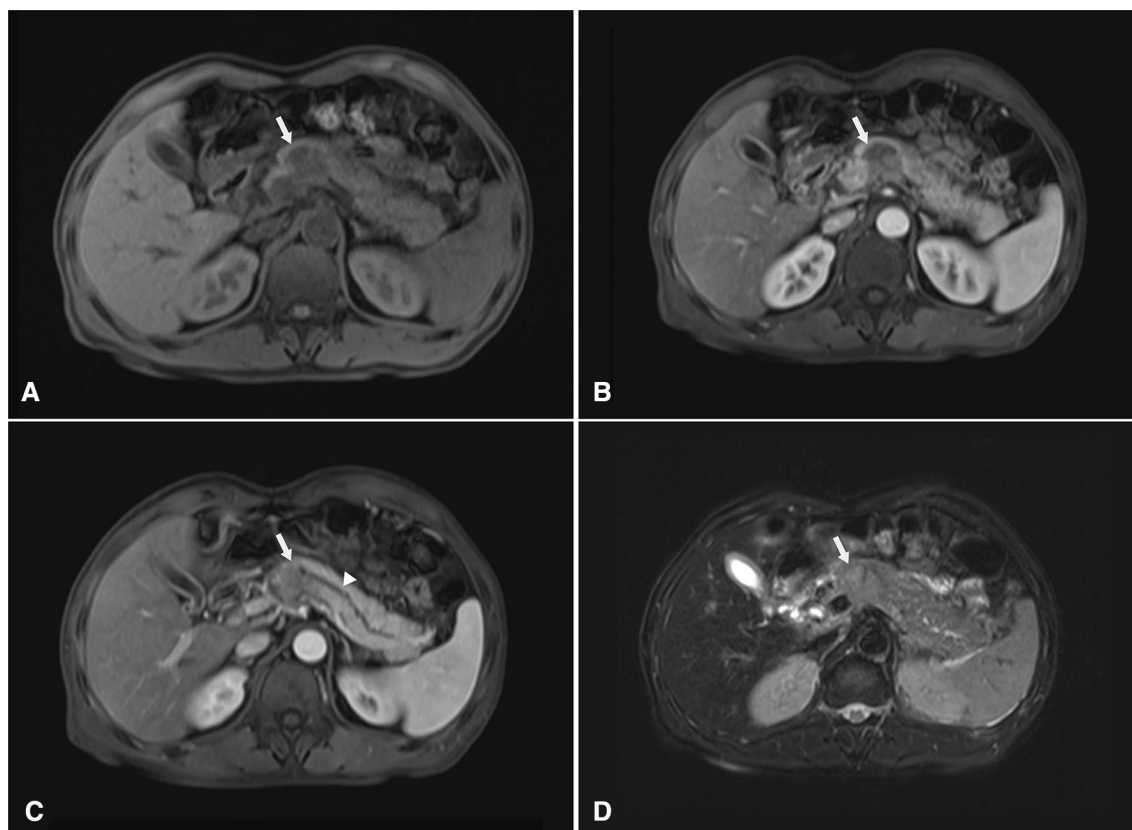
—

Fig. 3 Pancreatic neuroendocrine tumor in a 53-year-old man with LNM. **a** Axial T1-weighted image (T1WI) shows a well-defined hypointense tumor (white arrow) in the neck of the pancreas. **b**, **c** axial T1-weighted images obtained during arterial show non- hypervascularity lesion in the arterial phase accompanied by distal pancreatic duct dilatation (white arrowhead), **d** axial T2-weighted image (T2WI) shows a slight hyperintense lesion (white arrow)

(κ = 0.870, 0.855, respectively), and substantial agreement for presence of extrapancreatic tumor spread (κ = 0.797).

Discussion

In the current study, we have demonstrated that for patients with pNETs, non-enhancement characteristics and the presence of MPDD are independently associated with lymph node metastases at multivariate logistic regression analysis. Thus, MRI features may show better utility for predicting LNM of pNETs than clinicopathological parameters.

LNM is a significant prognostic predictor for pNETs [11, 12]. However, when considering that more extensive pancreatic resections can lead to higher complications, diverse surgical options are currently followed to treat pNETs [13]. Indeed, several recent studies have reported that lymphadenectomy should be strongly considered for surgical resection of pNETs, particularly for patients with a high risk of LNM [14]. Therefore, the preoperative prediction of the LNM in pNETs may help to avoid overtreatment and could be useful for surgical decisions.

Most previously published clinicopathological studies have shown the utility of tumor size in the prediction of LNM. Although Bettini et al. [15] reported that tumor size (> 2 cm) was significantly correlated with lymph node metastases, 14.4% of pNETs with LNM in the current study had primary tumor sizes $\leq$ 2 cm. Furthermore, Jiang et al. [16] demonstrated the tumor size difference between LNM-positive and LNM-negative groups of pNETs and suggested that the best threshold of tumor size for LNM be set at 2.5 cm. In contrast, Parekh et al. [17] and Gratian et al. [18] suggested that there was no difference in tumor size for pNETs with and without LNM. In our cohort, we similarly suggested that tumor size is not an independent risk predictor of LNM at multivariate logistic regression analysis. In addition, Postlewait et al. [19] found that male gender and head/uncinate location are associated with lymph node metastases; however, these parameters have not been generally consistent across many studies. Similarly, our results showed that there are no significant differences in gender, location, WHO classification, Ki-67 index, and type of function between the LNM-positive and LNM-negative groups. These results emphasize the

Table 4 Uni- and multivariate analyses of risk factors for LNM in pNETs

Risk factors	Univariate analysis			Multivariate analysis		
	OR	95% CI	P value	OR	95% CI	P value
Age (year)	1.007	0.974, 1.042	0.671			
Tumor margin (ill-define)	1.061	0.310, 3.624	0.925			
Location						
Head[a]						
Body	0.610	0.151, 2.468	0.488			
Tail	0.743	0.284, 1.945	0.546			
Tumor texture						
Cystic	7.200	0.622, 83.342	0.114			
Solid	2.779	0.333, 23.228	0.345			
Solid and cystic[a]						
Tumor size > 2 cm	9.867	2187, 44.514	0.003*	3.824	0.582, 25.126	0.163
Ki-67 > 5%	4.227	1.673, 10.682	0.002*	1.063	0.203, 5.557	0.942
Type of function (functioning)	3.138	0.674, 14.612	0.145			
Signal in T2-weighted images						
Hyperintense[a]						
Isointense	1.743	0.402, 7.548	0.458			
Hypointense	2.324	0.825, 6.549	0.111			
Histological classification						
G1[a]						
G2	4.587	1.240, 16.968	0.022*	1.063	0.174, 6.841	0.947
G3	11.333	2.209, 58.147	0.004*	0.277	0.015, 5.010	0.385
Non-enhancement pattern	8.000	2.992, 21.388	< 0.001*	6.652	1.369, 32.321	**0.019***
Signal on portal phase						
Hyperintense[a]						
Isointense	1.705	0.628, 4.630	0.296			
Hypointense	2.083	0.600, 7.233	0.248			
Signal on delay phase						
Hyperintense[a]						
Isointense	1.373	0.478, 3.941	0.556			
Hypointense	2.140	0.667, 6.869	0.201			
MPDD [present]	8.111	2.882, 22.825	< 0.001*	6.745	1.379, 32.991	**0.018***
Pancreatic atrophy [present]	3.200	1.105, 9.269	0.032*	1.021	0.262, 3.988	0.976
Extrapancreatic tumor spread [present]	5.308	2.001, 14.011	0.001*	0.797	0.178, 3.569	0.767
ADC ($\times 10^{-3}$mm^2/s)	0.131	0.042, 0.403	< 0.001*	0.257	0.059, 1.126	0.071
CNR during the arterial phase	0.262	0.103, 0.669	0.005*	0.936	0.185, 4.732	0.936
CNR during the portal phase	0.947	0.693, 0.995	0.047*	1.162	0.249, 5.422	0.849
CNR during the delay phase	0.213	0.045, 0.993	0.045*	1.267	0.099, 16.268	0.856

LNM lymph node metastasis, *OR* odds ratio, *CI* confidence interval, *ADC* apparent diffusion coefficient, *CNR* Contrast-to-noise ratio, *MPDD* main pancreatic duct dilation

*Statistically significant results from logistic regression analysis

[a]Data were used as the reference category

difficulty of identifying patients with pNETs at high risk for LNM solely by assessing clinical data.

Compared to indefinite clinicopathological predictors of LNM, in this mono-institutional study, we found two reliable independent radiological risk factors, including enhancement characteristics and MPDD, could preoperatively predict the LNM of pNETs. Indeed, several previously published studies have reported that hypoenhancing
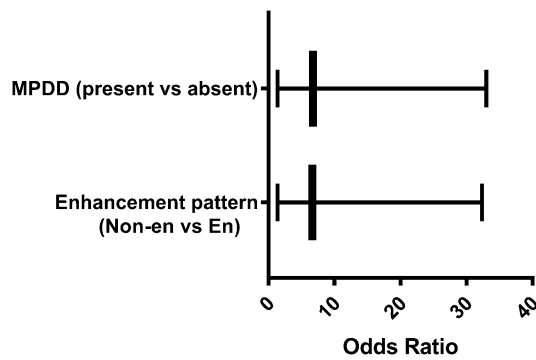
Fig. 4 Multivariate logistic regression analysis, probability of lymph node metastasis. Enhancement pattern and MPDD, were associated with increase in probability of lymph node metastasis (*P* values = 0.019 and 0.018, respectively). *Non-en* non-enhancement, *En* enhancement
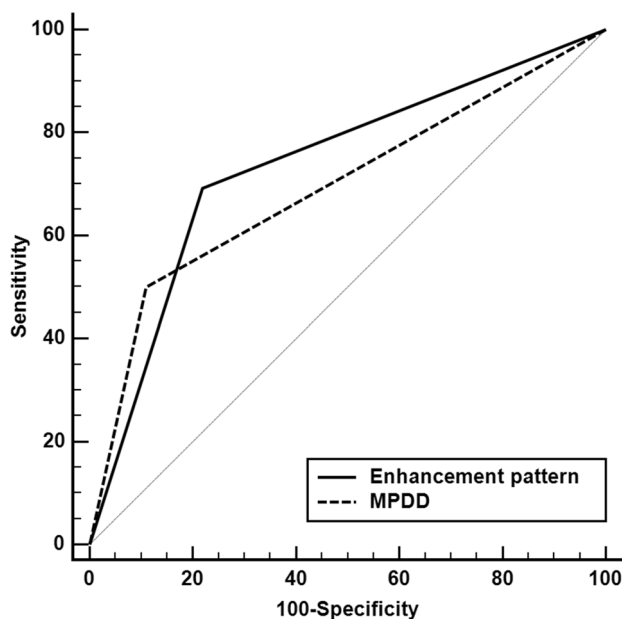

Fig. 5 ROC curve for differentiating LNM-positive and LNM-negative of pNETs using enhancement pattern and MPDD. The sensitivity, specificity, and area under the receiver operating characteristic curve of the non-enhancement pattern and MPDD were 69.23%, 78.05%, 0.736 and 50.00%, 89.02%, 0.695, respectively

pNETs are more likely to be high-grade pNETs [20–22]. In our study, non-enhancement pNETs more frequently presented with LNM, which may be explained, to some extent, by the association between non-enhancement characteristic and biological aggressiveness, similar to a recent study by Kim et al. [23] who used CT to predict the biological aggressiveness of pNETs. In addition, Takuya et al. [13] recently reported that tumor enhancement characteristics on contrast-enhanced computed tomography (CE-CT) are potential preoperative predictors of LNM of pNETs, which is similar to our results. The non-enhancement pattern,

therefore, may be considered a novel radiological factor for identifying candidates for regional lymph node dissection.

In our cohort, we also found that MPDD was significantly associated with LNM. pNETs with MPDD appeared to be more fibrotic and infiltrative into adjacent structures, which is likely the reason that the pNETs with MPDD are more likely to present with LNM. In addition, Nanno et al. [24] similarly reported that MPDD in pNETs may be a useful imaging sign to indicate nodal metastasis and tumor recurrence. From the above results, patients with a non-enhancement pattern and MPDD (even small in size < 2 cm) may benefit from extended lymph node dissection during surgery.

There were several limitations in our study. First, the retrospective nature of our study may have introduced inherent selection and verification biases. In addition, as we collected only surgically confirmed tumors, our study results may not represent the true status of LNM in pNETs. Second, this study was retrospective, performed at a single center, and enrolled a relatively small population of patients with pNETs. Third, the MR machines and protocols used in our research were variable, owing to the retrospective study. However, the primary MRI protocols used in our study were similar, and we excluded any MR images that were considered to be poor quality for analysis and prediction.

In conclusion, based on our findings, we identified MR features, including the non-enhancement pattern and MPDD, as noninvasive and reliable factors to predict LNM in pNETs. MRI features may be more effective predictors of LNM than clinicopathological predictors for pNETs. These radiological predictors are easily obtained preoperatively, and may help to avoid missing pNETs with a high risk of LNM and contribute to decision-making in the multidisciplinary treatment of these tumors.

Compliance with ethical standards

References

1. Kartalis N, Mucelli RM, Sundin A. (2015) Recent developments in imaging of pancreatic neuroendocrine tumors. Ann Gastroenterol 28: 193-202
2. Oberg K, Sundin A. (2016) Imaging of Neuroendocrine Tumors. Front Horm Res 45: 142-51
3. Rindi G, Kloppel G, Alhman H, et al. (2006) TNM staging of foregut (neuro)endocrine tumors: a consensus proposal including a grading system. Virchows Arch 449: 395-401
4. Jiang Y, Jin JB, Zhan Q, Deng XX, Shen BY. (2015) Impact and Clinical Predictors of Lymph Node Metastases in Nonfunctional Pancreatic Neuroendocrine Tumors. Chin Med J (Engl) 128: 3335-44
5. Hashim YM, Trinkaus KM, Linehan DC, et al. (2014) Regional lymphadenectomy is indicated in the surgical treatment of pancreatic neuroendocrine tumors (PNETs). Ann Surg 259: 197-203
6. De Robertis R, Maris B, Cardobi N, et al. (2018) Can histogram analysis of MR images predict aggressiveness in pancreatic neuroendocrine tumors? Eur Radiol 28: 2582-2591
7. Lotfalizadeh E, Ronot M, Wagner M, et al. (2017) Prediction of pancreatic neuroendocrine tumour grade with MR imaging features: added value of diffusion-weighted imaging. Eur Radiol 27: 1748-1759
8. Wang Y, Chen ZE, Yaghmai V, et al. (2011) Diffusion-weighted MR imaging in pancreatic endocrine tumors correlated with histopathologic characteristics. J Magn Reson Imaging 33: 1071-9
9. Jeon SK, Lee JM, Joo I, et al. (2017) Nonhypervascular Pancreatic Neuroendocrine Tumors: Differential Diagnosis from Pancreatic Ductal Adenocarcinomas at MR Imaging-Retrospective Cross-sectional Study. Radiology 284: 77-87
10. Nanno Y, Toyama H, Otani K, et al. (2016) Microscopic venous invasion in patients with pancreatic neuroendocrine tumor as a potential predictor of postoperative recurrence. Pancreatology 16: 882-7
11. Curran T, Pockaj BA, Gray RJ, et al. (2015) Importance of lymph node involvement in pancreatic neuroendocrine tumors: impact on survival and implications for surgical resection. J Gastrointest Surg 19: 152-60
12. Taki K, Hashimoto D, Nakagawa S, et al. (2017) Significance of lymph node metastasis in pancreatic neuroendocrine tumor. Surg Today 47: 1104-1110
13. Mizumoto T, Toyama H, Terai S, et al. (2017) Prediction of lymph node metastasis in pancreatic neuroendocrine tumors by contrast enhancement characteristics. Pancreatology 17: 956-961
14. Boninsegna L, Panzuto F, Partelli S, et al. (2012) Malignant pancreatic neuroendocrine tumour: Lymph node ratio and Ki67 are predictors of recurrence after curative resections. European Journal of Cancer 48: 1608-1615
15. Bettini R, Partelli S, Boninsegna L, et al. (2011) Tumor size correlates with malignancy in nonfunctioning pancreatic endocrine tumor. Surgery 150: 75-82
16. Jiang Y, Jin JB, Zhan Q, et al. (2015) Impact and Clinical Predictors of Lymph Node Metastases in Nonfunctional Pancreatic Neuroendocrine Tumors. Chin Med J (Engl) 128: 3335-44
17. Parekh JR, Wang SC, Bergsland EK, et al. (2012) Lymph node sampling rates and predictors of nodal metastasis in pancreatic neuroendocrine tumor resections: the UCSF experience with 149 patients. Pancreas 41: 840-4
18. Gratian L, Pura J, Dinan M, et al. (2014) Impact of extent of surgery on survival in patients with small nonfunctional pancreatic neuroendocrine tumors in the United States. Ann Surg Oncol 21: 3515-21
19. Postlewait LM, Ethun CG, Baptiste GG, et al. (2016) Pancreatic neuroendocrine tumors: Preoperative factors that predict lymph node metastases to guide operative strategy. J Surg Oncol 114: 440-5
20. Rodallec M, Vilgrain V, Couvelard A, et al (2006) Endocrine pancreatic tumours and helical CT: contrast enhancement is correlated with microvascular density, histoprognostic factors and survival. Pancreatology 6: 77-85
21. Worhunsky DJ, Krampitz GW, Poullos PD, et al. (2014) Pancreatic neuroendocrine tumours: hypoenhancement on arterial phase computed tomography predicts biological aggressiveness. HPB (Oxford) 16: 304-11
22. Hyodo R, Suzuki K, Ogawa H, et al. (2015) Pancreatic neuroendocrine tumors containing areas of iso- or hypoattenuation in dynamic contrast-enhanced computed tomography: Spectrum of imaging findings and pathological grading. Eur J Radiol 84: 2103-9
23. Kim JH, Eun HW, Kim YJ, et al. (2016) Pancreatic neuroendocrine tumour (PNET): Staging accuracy of MDCT and its diagnostic performance for the differentiation of PNET with uncommon CT findings from pancreatic adenocarcinoma. Eur Radiol 26: 1338-47
24. Nanno Y, Matsumoto I, Zen Y, et al. (2017) Pancreatic Duct Involvement in Well-Differentiated Neuroendocrine Tumors is an Independent Poor Prognostic Factor. Ann Surg Oncol 24: 1127-1133